Theoretical prediction of output performance of ^{63}NiO-Si heterojunction betavoltaic cell

Yu Wang, Renzhou Zheng, Jingbin Lu, et al.

View Online   Export Citation   CrossMark

ARTICLES YOU MAY BE INTERESTED IN

AIP Publishing

Theoretical prediction of output performance of ⁶³NiO-Si heterojunction betavoltaic cell

View Online   Export Citation   CrossMark

Yu Wang,[1] (iD) Renzhou Zheng,[1] (iD) Jingbin Lu,[1,a] (iD) Xiaoyi Li,[1] Ziyi Chen,[1] Xue Zhang,[1] Yuehui Zhang,[1] Lei Liang,[2,3,4]
Yugang Zeng,[2] Li Qin,[2] and Yumin Liu[5]

AFFILIATIONS

[1]College of Physics, Jilin University, Changchun 130012, China
[2]State Key Laboratory of Luminescence and Applications, Changchun Institute of Optics, Fine Mechanics and Physics,
 Chinese Academy of Sciences, Changchun 130033, China
[3]Center of Materials Science and Optoelectronics Engineering, University of Chinese Academy of Sciences, Beijing 100049, China
[4]Peng Cheng Laboratory, No. 2, Xingke 1st Street, Shenzhen 518000, China
[5]College of Nuclear Science and Engineering, East China University of Technology, Nanchang 330013, China

[a]Author to whom correspondence should be addressed: ljb@jlu.edu.cn

ABSTRACT

For the ⁶³NiO-Si heterojunction betavoltaic nuclear battery, the energy deposition of the energy conversion material itself was simulated by Monte Carlo simulation, and the structure of the ⁶³NiO-Si heterojunction was optimized based on the theoretical calculation results. When the thickness of ⁶³NiO is 4 μm and the doping concentration of Si is 1×10^{15} cm^{-3}, the short-circuit current density, open-circuit voltage, fill factor, and maximum output power density of the nuclear battery are 1.22 μA · cm^{-2}, 3.17 V, 0.95, 3.67 μW · cm^{-2}. In addition, the output performance of ⁶³Ni/NiO-Si heterojunction betavoltaic nuclear cell was calculated in this study. Under the condition that the activity of the radioactive source and the thickness of NiO(⁶³NiO) are the same in the two structures, the proposed structure (⁶³NiO-Si) has greatly improved the output performance of the nuclear battery by reducing the energy lost from radioactive source self-absorption.

Published under an exclusive license by AIP Publishing. https://doi.org/10.1063/5.0100186

Betavoltaic nuclear battery is a kind of device that convert decay energy into electric energy. It is mainly composed of a radioactive source and an energy converter. The cell has the advantages of long service life, strong anti-interference ability, small size, and so on. However, due to the self-absorption effect of radioactive sources in nuclear batteries, the decay energy of radioactive sources cannot be fully utilized in the energy converter. This has become a bottleneck in nuclear battery research. Many research groups have carried out discussions in an attempt to reduce the negative impact of the self-absorption of radioactive sources. In 2018, Alam *et al.* proposed a layered structure to optimize the thickness of a radioactive source by analyzing the self-absorption effect.[1] In 2020, Rahastama *et al.* believed that self-absorption and self-scattering were the main problems of energy loss of radioactive sources and investigated the influence of self-absorption of radioactive sources on each layer of semiconductor materials by changing the size of the radioactive source.[2] In 2019, Wu *et al.* found that the self-absorption of the silicon-based radioactive source was serious with the increase in the thickness of the radioactive source and selected the optimal thickness of the radioactive source by

simulating the emission energy spectrum of the radioactive source.[3] Subsequently, in 2020, this team proposed the use of layered structures to mitigate the effect of self-absorption of radioactive source on the output performance of nuclear battery.[4] In 2021, Yakimov *et al.* used ⁶³Ni and n-type β-Ga$_2$O$_3$ to compose a Schottky nuclear cell to reduce the energy of the radioactive source deposited in the Schottky metal.[5] It is clear that these research groups have achieved some positive results in reducing the self-absorption of radioactive sources but have not been applied to the energy deposited inside the radioactive sources themselves. However, the energy deposited inside the radioactive source is the main part of the energy loss.

In this research, we propose to make the radioactive source into a metal oxide to form a heterojunction with silicon. The metal oxide will be both a radioactive source and a role as an energy conversion material. The energy deposited in the metal oxide will also be used to generate electron–hole pairs. At the same time, we studied the relationship between the doping concentration and the thickness of the radioactive metal oxide and the output performance of the nuclear battery. The parameters in the theoretical calculations are mostly

derived from experimental studies to optimize the proposed structure. Furthermore, we compared the output performance of the proposed nuclear battery with the conventional nuclear battery. (The radioactive source is separated from the energy converter.) The results show that the output performance of the proposed nuclear battery is much higher than that of conventional nuclear battery.

As a first-generation semiconductor, silicon has been widely used in devices due to its mature manufacturing technology.[6–8] In order to form high-quality heterojunction, the metal oxide NiO is selected to form a heterojunction with silicon after considering the conductivity of the material and the lattice mismatch rate. NiO-Si heterojunction has been used in solar cells.[9–12] As the wideband gap semiconductor, nickel oxide (NiO), with a rock salt crystalline structure and a lattice constant of 4.17 Å, exhibits excellent chemical stability and interesting optical, electrical, and magnetic properties.[13] Moreover, NiO is one of few metal-oxide semiconductors showing a p-type conductivity and can be combined with an n-type semiconductor to fabricate a pn diode.[14,15] In this study, the nickel atom in NiO is replaced with radioactive ^{63}Ni, that is, a radioactive metal oxide is formed. The output performance of the ^{63}NiO-Si heterojunction nuclear battery is calculated, and the influence of the thickness of ^{63}NiO and the doping concentration of Si on the performance of the nuclear battery is analyzed. The output performance of ^{63}NiO-Si will be significantly better than that of the conventional device (^{63}Ni/NiO-Si nuclear battery).

Figure 1(a) shows the physical model established in Monte Carlo simulation in which the surface area of the ^{63}NiO is 1×1 cm^2. The semiconductor heterojunction diode is $1\,\text{cm} \times 1\,\text{cm} \times 30\ \mu\text{m}$. The thickness of ^{63}NiO is variable, and the rest is the thickness of Si. As shown in Fig. 1(b), W_p and W_n are depletion layers in ^{63}NiO and Si, respectively. In order to facilitate the calculation of the output performance, the ^{63}NiO-Si structure is divided into five parts, these five parts are divided according to the generation rate and collection efficiency of electron–hole pairs, X_1 is the distance from the ^{63}NiO interface to its middle, and d_n is the thickness of p-^{63}NiO.

For p-n type heterojunction, due to the difference of energy band structure between the two materials, conduction band discontinuity (ΔE_c) and valence band discontinuity (ΔE_v) will be formed at the

FIG. 1. (a)The physical model established in Monte Carlo simulation. (b) Structure of the ^{63}NiO-Si heterojunction betavoltaic cell.

conduction band and valence band potential barrier. For ^{63}NiO-Si heterojunction, conduction band discontinuity is 0.7 eV, and valence band discontinuity is 3.15 eV.[16] The built-in potential difference formed near the barrier can be obtained by the following formula:[17]

$$V_{bi} = -\Delta E_v + \frac{kT}{q}\ln\left(\frac{P_{p0}N_{vn}}{P_{n0}N_{vp}}\right), \tag{1}$$

$$P_{n0} = \frac{n_i^2}{N_d}, \tag{2}$$

where k is the Boltzmann constant, T is the absolute temperature (in this study, T is 300 K), and q is the electron charge. N_{vp} and N_{vn} are the effective valence band state densities of ^{63}NiO and Si (N_{vp} is 1×10^{19} cm^{-3}, N_{vn} is 1.04×10^{19} cm^{-3}), respectively. The width of the depletion layer formed by the diffusion of most carriers can be calculated according to the following formulas:[18]

$$W_n = \sqrt{\frac{2\epsilon_1\epsilon_2 N_a}{qN_d(\epsilon_1 N_d + \epsilon_2 N_a)}V_{bi}}, \tag{3}$$

$$W_p = \sqrt{\frac{2\epsilon_1\epsilon_2 N_d}{qN_a(\epsilon_1 N_d + \epsilon_2 N_a)}V_{bi}}, \tag{4}$$

$$W = W_n + W_p, \tag{5}$$

where ϵ_1 and ϵ_2 are the dielectric constants of ^{63}NiO and Si ($\epsilon_1 = 10.7$ and $\epsilon_1 = 11.7$).[17,19] On both sides of the depletion layer is the minority carrier diffusion length region, which is conducive to minority carrier collection. When the doping concentration (N_a) of ^{63}NiO is 1×10^{18} cm^{-3}, the minority carrier lifetime τ_n of p-type ^{63}NiO is 92×10^{-6} s, and the diffusion coefficient D_n is 12 cm$^2 \cdot$ s^{-1},[15] the minority diffusion length (L_n) of ^{63}NiO side and the minority diffusion length (L_p) of Si can be obtained by the following formulas:[20]

$$L_n = \sqrt{D_n \tau_n}, \tag{6}$$

$$L_p = \sqrt{\frac{kT}{q} \times \frac{\left\{130 + \dfrac{370}{1+\left(\dfrac{N_d}{8\times10^{17}}\right)^{1.25}}\right\}}{7.8 \times 10^{-13}N_d + 1.8 \times 10^{-31}N_d^2}}. \tag{7}$$

The reverse saturation current density can be calculated from formula (8),[21] where d_n is the thickness of the ^{63}NiO and d_p is the thickness of the Si. φ can be obtained by formula (9), where s is the surface recombination rate (it is set to 10^6 cm $\cdot$ s^{-1}),

$$J_0 = q\left\{\frac{N_d D_n \exp[-q(V_{bi} - \Delta E_c)/kT]}{L_n \tan h(d_n/L_n)} \right. \\ \left. + \frac{N_a D_p \exp[-q(V_{bi} + \Delta E_v)/kT]}{L_p \tan h(d_p/L_p + \varphi)}\right\}, \tag{8}$$

$$\tan h\varphi = \frac{sL_p}{D_p}. \tag{9}$$

The reverse saturation current density is related to the thickness of ^{63}NiO, minority carrier diffusion length, and mobility. It can be seen from Fig. 2 that the reverse saturation current density increases as the thickness of ^{63}NiO decreases. The reverse saturation current is formed by the diffusion of minority carriers. When the doping concentration of
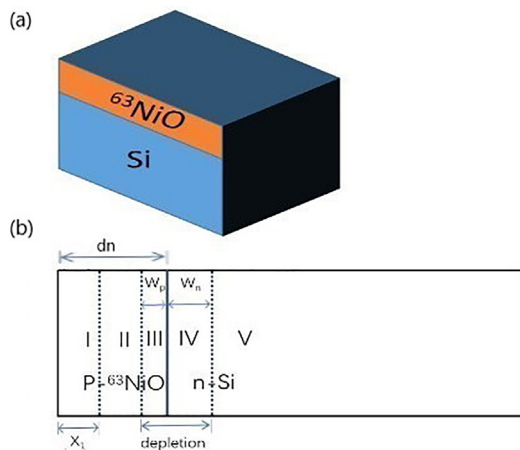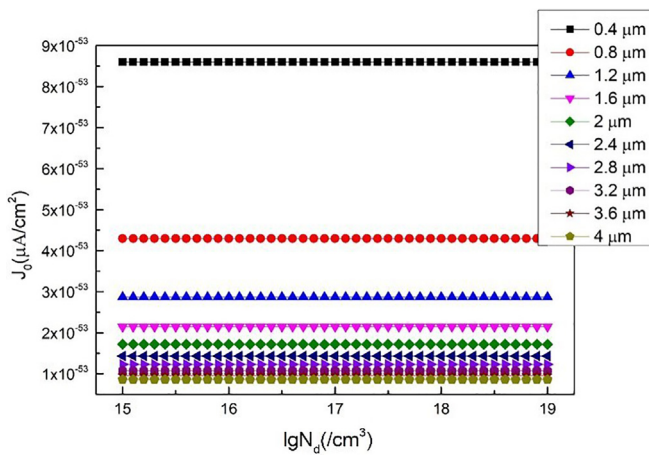
FIG. 2. The reverse saturation current density (J_0) vs the doping concentration (N_d) for different ^{63}NiO thicknesses.

Si is determined, the reverse saturation current is mainly affected by minority carrier diffusion and mobility. With the decrease in the thickness of ^{63}NiO, the diffusion equilibrium is easier to achieve, and the reverse saturation current density is larger. The influence of minority carrier diffusion length and mobility on reverse saturation current density gradually decreases with the increase in ^{63}NiO thickness. When the doping concentration is changed and the thickness of ^{63}NiO is determined, the reverse saturation current density is almost negligibly affected by the minority carrier diffusion length and mobility.

When β particles are incident into an energy converter, a large number of electron–hole pairs will be generated by ionization interaction. Under the built-in electric field, electrons and holes move to the two electrodes to form the current. The energy deposition can be obtained through Monte Carlo simulation, and the relationship between deposition power and incident depth can be obtained through the data processing. The data processing method is as follows: We obtained the relationship between total energy deposition and incidence depth through Monte Carlo simulation and then multiplied the activity of the radioactive source (that is, the number of particles emitted per unit time), the relationship between the deposition power and

the incident depth can be obtained. Different from conventional device, the formula fitting of the generation rate of electron–hole pairs is more complicated in ^{63}NiO-Si. Since the energy conversion material is radioactive, the variation of energy deposition with depth in the energy converter is no longer a simple exponential decay law. For conventional device, the maximum energy is deposited on the surface of the energy converter and then decreases with the increase in depth. For the ^{63}NiO-Si, the most energy is deposited in the middle of ^{63}NiO. The expression of the generation rate of the electron–hole pair with incident depth as shown in the following formula:[22]

$$G(x) = \begin{cases} \dfrac{G_1}{q\varepsilon_{NiO}}\exp(\alpha_1 x), & 0 < x < d_n/2, \\[2mm] \dfrac{G_2}{q\varepsilon_{NiO}}\exp(-\alpha_2(x - d_n/2)), & d_n/2 < x < d_n, \\[2mm] \dfrac{G_3}{q\varepsilon_{Si}}\exp(-\alpha_3(x - d_n)), & d_n < x < 30, \end{cases} \quad (10)$$

where G_1, G_2, and G_3 are the generation rates of electron–hole pairs and α_1, α_2, and α_3 are the absorption coefficients. Those parameters are given in Table I. ε is the average ionization energy, which can be given by the following formula, in which E_g is the bandgap (for ^{63}NiO, it is 3.8 eV; for Si, it is 1.12 eV),[17,19]

$$\varepsilon = 2.8E_g + 0.5. \quad (11)$$

The electron–hole pairs generated in the depletion layer region will be directly separated and moved to electrodes, and the electron–hole pairs generated in the minority diffusion length region will be moved to the depletion layer by diffusion and then separated. The collection efficiency of electron-hole pairs in different regions of the energy conversion material is different, which can be obtained from the following formula,[3] where $d(x)$ is the distance from position x to the depletion layer and L is the length of minority diffusion:

$$CE(x) = 1 - \tan h\left(\frac{d(x)}{L}\right). \quad (12)$$

Those electrons and holes are collected by the electrodes on both sides of the battery and output to form a current. The current can be

TABLE I. The parameters of the generation rate of electron–hole pairs and absorption coefficients.

The thickness of NiO (μm)	G_1 (cm$^{-3}\cdot$s^{-1})	G_2 (cm$^{-3}\cdot$s^{-1})	G_3 (cm$^{-3}\cdot$s^{-1})	α_1 (cm^{-1})	α_2 (cm^{-1})	α_3 (cm^{-1})
0.4	6236.64	15 572.93	1960.83	16 794.97	20 216.71	5028.09
0.8	9567.74	23 579.99	3124.7	10 948.32	9473.38	4799.85
1.2	12 504.87	36 993.398	3759.96	6803.52	8807.95	4699.95
1.6	14 449.85	42 411.5	4180.74	5399.998	6604.09	4645.26
2	15 573.64	46 048.42	4371.6	4906.63	5173.98	4553.75
2.4	17 113.37	57 070.6	4555.87	3656.70	5077.45	4515.232
2.8	17 166.59	56 445.33	4887.07	3238.98	4052.07	4695.04
3.2	18 537.9	56 928.42	4939.34	2923.96	3427.36	4659.75
3.6	19 148.89	56 822.52	4958.94	2623.136	2928.996	4634.52
4	19 674.44	56 198.92	4850.7	2373.274	2520.696	4550.389

obtained from the following formulas,[3] where d_p is the thickness of Si and the parameters can be obtained from Table I:

$$j_1 = \int_0^{X_1} \frac{G_1 \exp(\alpha_1 x)}{\varepsilon_{^{63}NiO}} \left(1 - \tan h\left(\frac{d_n - W_p - x}{L_n}\right) \right) dx, \quad (13)$$

$$j_2 = \int_{X_1}^{d_n - W_p} \frac{G_2 \exp(-\alpha_2 x)}{\varepsilon_{NiO}} \left(1 - \tan h\left(\frac{d_n - W_p - x}{L_n}\right) \right) dx, \quad (14)$$

$$j_3 = \int_{d_n - W_p}^{d_n} \frac{G_2 \exp(-\alpha_2 x)}{\varepsilon_{NiO}} dx, \quad (15)$$

$$j_4 = \int_0^{W_n} \frac{G_3 \exp(-\alpha_3 x)}{\varepsilon_{Si}} dx, \quad (16)$$

$$j_5 = \int_{W_n}^{L_p - d_p} \frac{G_3 \exp(-\alpha_3 x)}{\varepsilon_{Si}} \left(1 - \tan h\left(\frac{x - W_n}{L_p}\right) \right) dx, \quad (17)$$

$$J_{sc} = j_1 + j_2 + j_3 + j_4 + j_5. \quad (18)$$

Figure 3(a) shows the relationship between the short-circuit current density of each part and the doping concentration of silicon when the thickness of ^{63}NiO is 0.4 and 4 μm, respectively. The short-circuit current density of the three parts contributed by ^{63}NiO($j_1.j_2.j_3$) does not change significantly with the increase in doping concentration. j_3 is the current contributed by the depletion layer in ^{63}NiO, which is expected to obtain a high current. However, when the doping concentration of ^{63}NiO is determined, the width of the depletion layer (W_p) is very small, so that the current formed by the separation of electron– hole pairs is very small. The short-circuit current density in the depletion layer region of silicon (j_4) gradually decreases, because the decrease in the depletion layer width affects the collection of carriers in this region. The short-circuit current density contributed by the minority carrier diffusion length region in silicon (j_5) increases first and then decreases. The reason is that as the width of the depletion layer decreases, the energy collected in the minority carrier diffusion length region increases, which leads to an increase in current; as the doping concentration continues to increase, the minority carrier diffusion length begins to decrease, resulting in a decrease in current. The short-circuit current density of each part in Fig. 3(b) has the same trend with the change in doping concentration. By comparing the two figures, it can be found that as the thickness of ^{63}NiO increases, the short-circuit current density increases, and the short-circuit current density contributed by ^{63}NiO also increases significantly.

As shown in Fig. 4(a), the short-circuit current density increases with the increase in thickness of ^{63}NiO. The reason is that the increase in the thickness of ^{63}NiO is actually increased the activity of radioactive sources, the depletion layer width and minority diffusion length unchanged. The increase in the activity of the radioactive source will increase the electron–hole pairs generated in the energy converter and, thus, increase the short-circuit current density. However, it should be mentioned that high beta absorptivity may lead to a reduction in local resistivity in real device fabrication. (In the process of theoretical calculation, the relevant factors, such as Ohmic contact, temperature, and the influence of vacuum on the nuclear battery, have not been considered). With the increase in doping concentration of Si, the influence on the short-circuit current density is small. The doping concentration of silicon has little effect on the trend of the short-circuit current
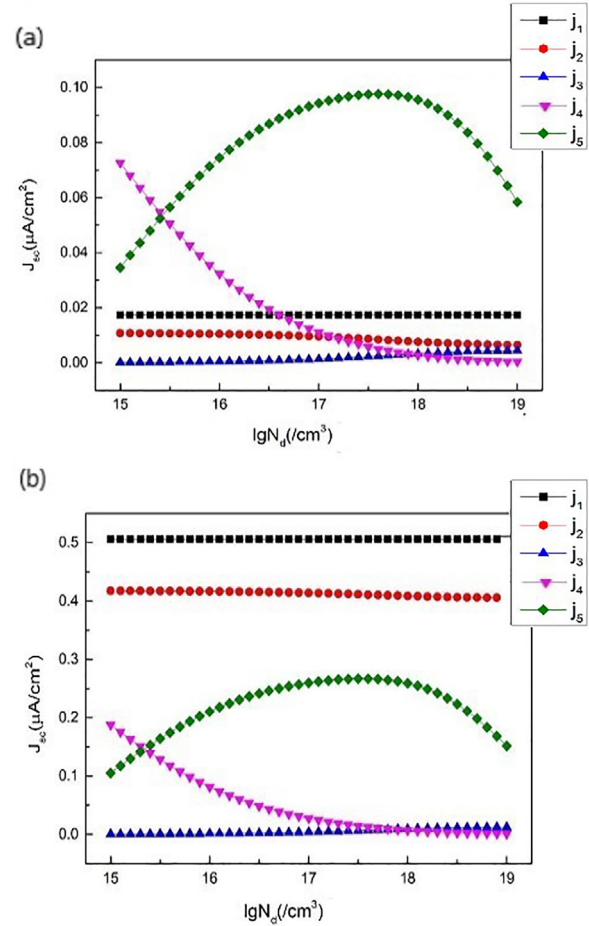

FIG. 3. (a) The short-circuit current density contributed by each part (j_1, j_2, j_3, j_4, j_5) vs the doping concentration(N_d) for 0.4 μm ^{63}NiO. (b) The short-circuit current density contributed by each part (j_1, j_2, j_3, j_4, j_5) vs the doping concentration (N_d) for 4 μm ^{63}NiO.

density. The increase in doping concentration of silicon will mainly reduce the depletion layer width and minority carrier diffusion length to adversely affect the carrier collection,

$$V_{oc} = \frac{kT}{q} \ln\left(\frac{J_{sc}}{J_0} + 1\right), \quad (19)$$

$$FF = \frac{v_{oc} - \ln(v_{oc} + 0.72)}{v_{oc} + 1} \quad v_{oc} = \frac{qV_{oc}}{kT}, \quad (20)$$

$$P_{max} = J_{sc} V_{oc} FF. \quad (21)$$

The formulas of open-circuit voltage, filling factor, and maximum output power density are shown in (19)–(21).[23] As shown in Fig. 4(b), the open-circuit voltage and filling factor have basically the same relationship with the thickness of ^{63}NiO and the doping concentration of Si, which are mainly affected by short-circuit current and reverse saturation current. With the increase in the thickness of ^{63}NiO, the open-circuit voltage increases gradually, and the increasing trend gradually decreases due to the influence of reverse saturation current.
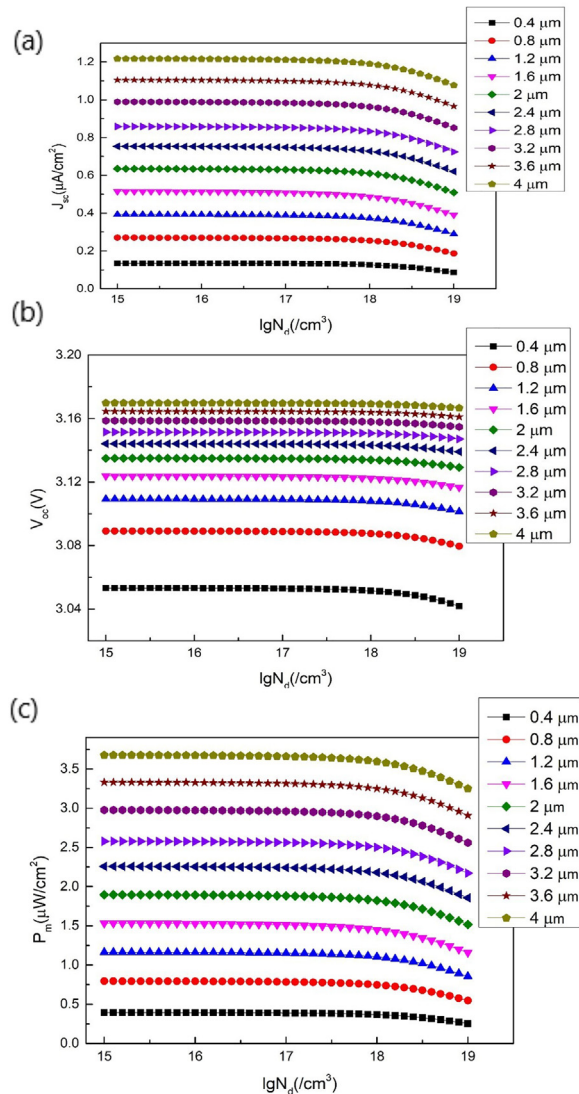
FIG. 4. (a) The short-circuit current density (J_{sc}) vs the doping concentration (N_d) for different ^{63}NiO thicknesses. (b) The open-circuit voltage (V_{oc}) vs the doping concentration (N_d) for different ^{63}NiO thicknesses. (c) The maximum output power density (P_{max}) vs the doping concentration (N_d) for different ^{63}NiO thicknesses.

FIG. 5. (a) The proposed structure. (b) The conventional structure.

Figure 4(c) shows that the maximum output power density of the nuclear battery reaches the maximum value when the thickness of ^{63}NiO is 4 μm.

Moreover, the output performance of the nuclear battery with the conventional structure was also calculated in this study. Figure 5(a) shows the proposed structure. Figure 5(b) shows the conventional structure widely used in the study of nuclear batteries in which the radioactive source of nuclear batteries is separated from the energy converter. For conventional device, the calculation method mentioned in Ref. 3. The thickness of the energy converter of both structures is 30 μm to ensure that as much energy as possible is deposited in the device. The thickness of ^{63}NiO and NiO is constantly changed and
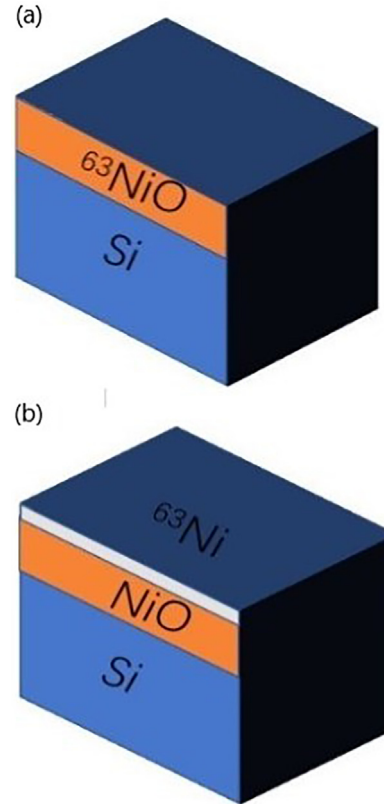
always the same. The corresponding thickness of ^{63}Ni will also be constantly changed. As the thickness of ^{63}NiO in the proposed device changes, the corresponding ^{63}Ni activity in the conventional device is changed in order to keep the activity of the radioactive source consistent with that of the proposed structure.

Figure 6 shows the comparison results of the output performance of the two structures. As shown in Fig. 6(a), as the thickness of NiO increases, the short-circuit current density increases for both the proposed device and the conventional device. However, as the activity of the radioactive source increases, the gap between the short-circuit current density of the proposed device and that of conventional devices gradually widens. The reason is that as the thickness of NiO(^{63}NiO) increases, the self-absorption effect of the radioactive source has a greater negative impact on conventional device, and more energy is deposited in the radioactive source. As shown in Figs. 6(b) and 6(c), since the proposed device and the conventional device do not change the band structure of the energy converter, the difference in open-circuit voltage is not large. The fill factor has the same trend as the open-circuit voltage. Finally, Fig. 6(d) shows that the maximum output power density of the proposed nuclear battery is significantly higher than that of conventional nuclear battery. The reason is that the proposed structure has a higher electron–hole pair generation rate and carrier collection efficiency due to the reduced self-absorption effect of the radioactive source.
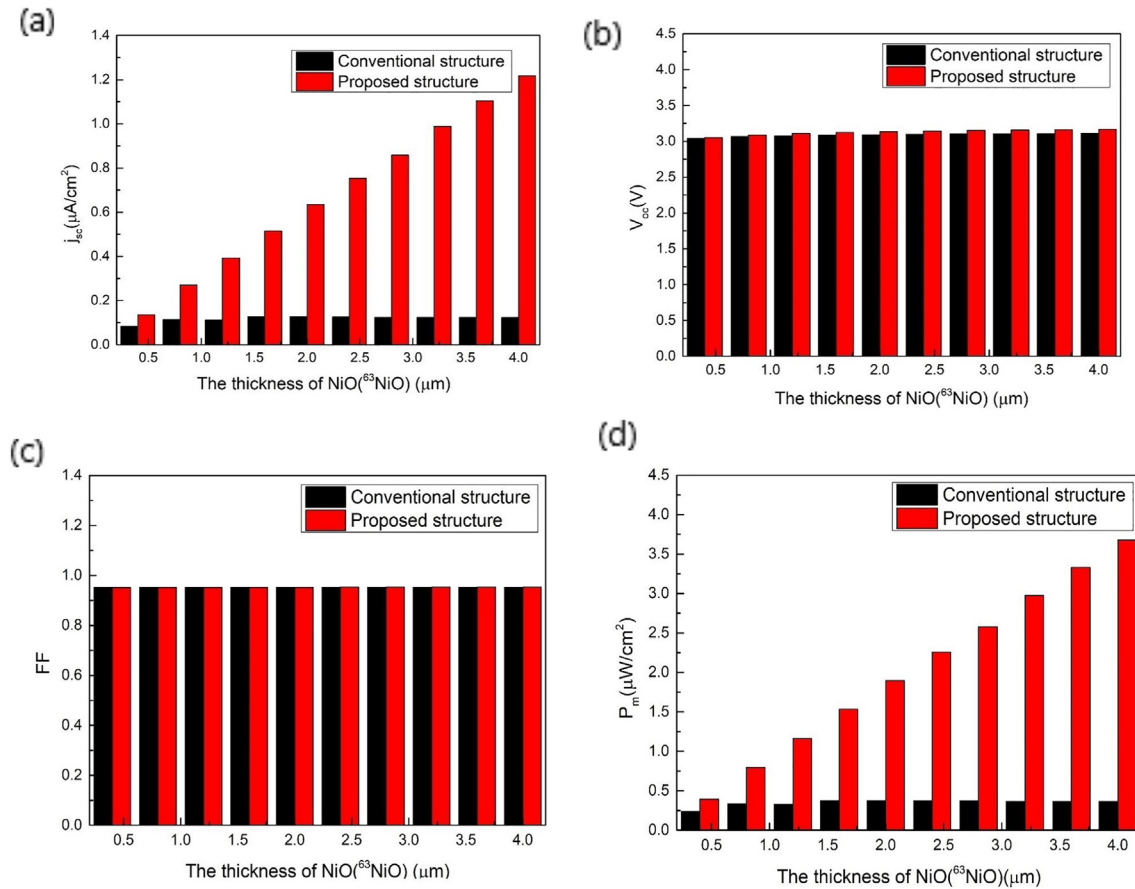
FIG. 6. The comparison results of the output performance for the two structures. (a) The short-circuit current density (J_{sc}) vs the thickness of NiO(^{63}NiO). (b) The open-circuit voltage (V_{oc}) vs the thickness of NiO(^{63}NiO). (c) The fill factor (FF) vs the thickness of NiO(^{63}NiO). (d) The maximum output power density (P_{max}) vs the thickness of NiO(^{63}NiO).

In order to reduce the negative effect of self-absorption of radioactive source on nuclear cell, the output performance of the integrated ^{63}NiO-Si heterojunction nuclear cell was calculated and optimized. The energy converter surface area is $1\,cm^2$. When the thickness of ^{63}NiO is 4 μm and the doping concentration of silicon is 1×10^{15} cm^{-3}, the short-circuit current, open-circuit voltage, filling factor, and maximum output power of the nuclear cell are 1.22 μA, 3.17 V, 0.95, and 3.67 μW, respectively. By simulating the output performance of conventional devices, when the thickness of ^{63}Ni is 0.95 μm, the thickness of NiO is 1.6 μm, and the doping concentration of silicon is 1×10^{15} cm^{-3}, the battery has the best electrical output performance. The short-circuit current, open-circuit voltage, filling factor, and the maximum output power of conventional nuclear cell are 0.126 μA, 3.087 V, 0.95, and 0.373 μW, respectively. Compared with the proposed device under the same thickness of ^{63}NiO, the output performance of the conventional device is much lower. When the thickness of ^{63}NiO is 4 μm, the thickness of NiO of the conventional device is also 4 μm, and the doping concentration (N_d) is 1×10^{15} cm^{-3}, the short-circuit current, open-circuit voltage, filling factor, and maximum output power of conventional devices are 0.123 μA, 3.11 V, 0.952, and

0.364 μW, respectively. By comparison, the maximum output power density of the proposed device is about 10 times that of the conventional device. What is more, the calculation method in this paper is also applicable to the other radioactive metal oxide heterojunctions, such as AlGaAs/GaAs, GaP/Si through doping to form radioactive metal oxide heterojunctions.

AUTHOR DECLARATIONS
Conflict of Interest

The authors have no conflicts to disclose.

Author Contributions

Yu Wang: Data curation (lead); Formal analysis (lead); Investigation (equal); Writing – original draft (lead). **Li Qin:** Resources (equal).

Yumin Liu: Resources (equal). **Renzhou Zheng:** Investigation (equal); Writing – review and editing (equal). **Jing-Bin Lu:** Resources (lead); Writing – review and editing (equal). **XiaoYi Li:** Writing – review and editing (equal). **Ziyi Chen:** Investigation (equal); Writing – review and editing (equal). **Xue Zhang:** Investigation (equal); Writing – review and editing (equal). **Yuehui Zhang:** Investigation (equal); Writing – review and editing (equal). **Lei Liang:** Resources (equal). **Yugang Zeng:** Resources (equal).

DATA AVAILABILITY

The data that support the findings of this study are available from the corresponding author upon reasonable request.

REFERENCES

[1]T. R. Alam, M. G. Spencer, M. A. Prelas, and M. A. Pierson, "Design and optimization of radioisotope sources for betavoltaic batteries," Int. J. Energy Res. **42**(7), 2564–2573 (2018).

[2]S. Rahastama, I. Agani, R. Salim, Y. C. Teluma, and A. Waris, "The investigation of self-absorption effect in cylindrical Ni-63/4H-SiC betavoltaic," J. Phys.: Conf. Ser. **1763**(1), 012057 (2021).

[3]M. Wu, S. M. Wang, Y. Ou, and W. B. Wang, "Optimization design of betavoltaic battery based on titanium tritide and silicon using Monte Carlo code," Appl. Radiat. Isot. **142**, 22–27 (2018).

[4]M. Wu and J. W. Zhang, "Design and simulation of high conversion efficiency betavoltaic battery based on a stacked multilayer structure," AIP Adv. **9**(7), 075124 (2019).

[5]E. B. Yakimov, A. Y. Polyakov, and S. J. Pearton, "Betavoltaic cell based on Ni/β-Ga$_2$O$_3$ and ^{63}Ni source," J. Vac. Sci. Technol. A **40**(1), 010401 (2022).

[6]J. W. Murphy, C. D. Frye, R. A. Henderson, M. A. Stoyer, L. F. Voss, and R. J. Nikoli, "Demonstration of a three-dimensionally structured betavoltaic," J. Electron. Mater. **50**(3), 1380–1385 (2021).

[7]A. A. Svintsov, A. A. Krasnov, M. A. Polikarpov, A. Y. Polyakov, and E. B. Yakimov, "Betavoltaic battery performance: Comparison of modeling and experiment," Appl. Radiat. Isot. **137**(1), 184–189 (2018).

[8]Y. Lei, Y. Yang, G. Li, Y. Liu, J. Xu, X. Xiong, S. Luo, and T. Peng, "Demonstration and aging test of a radiation resistant strontium-90 betavoltaic mechanism," Appl. Phys. Lett. **116**(15), 153901–153904 (2020).

[9]K. S. Khashan, J. A. Saimon, A. A. Hadi, and R. O. Mahdi, "Influence of laser energy on the optoelectronic properties of NiO/Si heterojunction," J. Phys.: Conf. Ser. **1795**(1), 012026 (2021).

[10]S. Thamri, M. H. Raouadi, and H. Ezzaouia, "Study of the performance of a ZnO-NiO/Si nanocomposite-based solar cell," ECS J. Solid State Sci. Technol. **9**(12), 125005 (2020).

[11]B. Parida, S. Kim, M. Oh, S. Jung, M. Baek, J.-H. Ryou, and H. Kim, "Nanostructured-NiO/Si heterojunction photodetector," Mater. Sci. Semicond. Process. **71**, 29–34 (2017).

[12]X. L. Yang, J. X. Guo, Y. Zhang, W. Liu, and Y. Sun, "Hole-selective NiO:Cu contact for NiO/Si heterojunction solar cells," J. Alloys Compd. **747**, 563–570 (2018).

[13]W. C. Lee, E. C. Choi, and J.-H. Boo, "A study on characterization of nano-porous NiO thin film to improve electrical and optical properties for application to automotive glass," Thin Solid Films **641**, 28–33 (2017).

[14]M. L. Grilli, S. Aydogan, and M. Yilmaz, "A study on non-stoichiometric p-NiO/n-Si heterojunction diode fabricated by RF sputtering: Determination of diode parameters," Superlattices Microstruct. **100**, 924–933 (2016).

[15]D. B. Patel, H.-S. Kim, M. Patel, K. R. Chauhan, J. E. Park, D. Lim, and J. Kim, "Front surface field formation for majority carriers by functional p-NiO layer employed Si solar cell," Appl. Phys. Lett. **109**(13), 133902–133905 (2016).

[16]I. Hotovy, J. Huran, L. Spiess, H. Romanus, D. Buc, and R. Kosiba, "NiO-based nanostructured thin films with Pt surface modification for gas detection," Thin Solid Films **515**(2), 658–661 (2006).

[17]D. A. Neamen, *Semiconductor Physics and Devices: Basic Principles*, 4th ed. (Publishing House of Electronics Industry, 2011).

[18]H. J. Hovel, *Semiconductors and Semimetals* (Academic Press, 1975).

[19]M. Hossain, F. H. Alharbi, and N. Tabet, "Copper oxide as inorganic hole transport material for lead halide perovskite based solar cells," Sol. Energy **120**, 370–380 (2015).

[20]B. L. Anderson, *Fundamentals of Semiconductor Devices* (McGraw-Hill Higher Education, Boston, 2005), pp. 83–120.

[21]A. G. Milnes, *Heterojunctions and Metal Semiconductor Junctions* (Academic Press, 1972).

[22]G. R. Ghasemi Nejad, F. Rahmani, and G. R. Abaeiani, "Design and optimization of beta-cell temperature sensor based on (63)Ni-Si," Appl. Radiat. Isot. **86**, 46–51 (2014).

[23]H. Guo and A. Lal, "Nanopower betavoltaic microbatteries," in *Proceedings of the 12th International Conference on Solid-State Sensors, Actuators and Microsystems* (IEEE, 2003), pp. 36–39.